Optics & Laser Technology 203 (2026) 115643

Contents lists available at ScienceDirect

Optics and Laser Technology

journal homepage: www.elsevier.com/locate/optlastec

Full length article

Ultra-narrow linewidth measurement of laser based on mutation particle swarm optimization of Voigt spectrum iteration process

Hongren Li [a,b], Ningmu Zou [c], Tian Xiao [a,b], Nasheeta Mazhar [a,b], Yixin Zhang [a,b,*], Jiaqi Ma [a,b], Xinyu Wang [a,b], Xuping Zhang [a,b,*], Erming Liang [a]

[a] College of Engineering and Applied Sciences, Nanjing University, Nanjing 210046, China
[b] Key Laboratory of Intelligent Optical Sensing and Manipulation, Ministry of Education, Nanjing University, Nanjing 210093, China
[c] School of Integrated Circuits, Nanjing University, Suzhou 215163, China

ARTICLE INFO

Keywords:
Ultra-narrow Linewidth Laser(UNLL)
Voigt Profile Fitting
LaserLinewidthMeasurement
Mutation Particle Swarm Optimization-Voigt (MPSO-Voigt)

ABSTRACT

The Voigt spectral fitting method, widely used for linewidth measurement of ultra-narrow linewidth laser (UNLL), exhibits significant measurement errors when determining the effective linewidth. This is because the method relies on the −20 dB linewidth of the self-heterodyne spectrum (SHS) obtained from the delayed self-heterodyne interferometer (DSHI) as the initial iteration value, which is susceptible to disturbance from shot noise. Here, we propose Mutation Particle Swarm Optimization-Voigt (MPSO-Voigt). It avoids initial value dependency through parallel particle swarm search, prevents premature convergence using mutation factors and dynamic inertia weights, simplifying complexity by incorporating Voigt-Lorentzian-Gaussian linewidth relationships. Numerical simulation show that compared to the traditional Voigt method, when the intrinsic linewidth of SHS is 100 Hz and the relative noise is 1 dB, the linewidth measurement error is reduced from 178% to 42% and the measurement fluctuation is decreased from 47% to 7%. Physical experiments on lasers with intrinsic linewidth $<$ 100 Hz show that the proposed MPSO-Voigt method can significantly suppress the influence of shot noise: the measured average effective linewidth is 97 Hz lower than the traditional Voigt method, and the fluctuation of linewidth measurement results is reduced by about 75%, which is close to numerical simulation. In addition, comparison with the FN-PSD method combined with the β-separation line criterion shows consistent linewidth results, further supporting the reliability of the proposed method. In summary, the MPSO-Voigt algorithm breaks the initial value dependence and noise sensitivity constraints of traditional Voigt method, realizing reliable and precise linewidth characterization for UNLL.

1. Introduction

Ultra-narrow Linewidth Laser (UNLL) hold significant importance in the application of high-precision coherent optical fiber sensing and high-speed coherent communication[1,2]. With the continuous advancement of laser linewidth compression techniques, commercial lasers with sub-kilohertz linewidth have become readily available[3,4]. The emergence and progression of UNLLs necessitate corresponding high-precision linewidth measurement technology.The intrinsic linewidth of a laser is determined by the design of its gain medium and resonator[5]. However, in practical operation, its effective linewidth is significantly broader than the intrinsic linewidth due to noise disturbances induced by factors such as optical phase fluctuations[6], mechanical vibrations, and temperature variations[7,8]. Therefore, the effective linewidth is often used as a critical metric for evaluating the stability and practical utility of a laser. In fiber-optic communication or sensing systems, the effective linewidth directly impacts the accuracy of phase signal extraction[9], making the precise measurement of the effective linewidth crucial for the practical application of UNLLs.

Laser linewidth measurement becomes increasingly challenging as the linewidth decreases, because higher spectral resolution and better system stability are required. Owing to their limited resolution, optical spectrometers generally resolve linewidths at the GHz level, while Fabry–Pérot interferometry can extend the measurable range to the MHz level[10]. For extremely narrow linewidth lasers, reference-cavity- or reference-laser-based methods can provide high measurement sensitivity, but they usually require additional frequency references, strict environmental isolation, and complex optical configurations. Therefore,

* Corresponding authors.
E-mail addresses: zyixin@nju.edu.cn (Y. Zhang), xpzhang@nju.edu.cn (X. Zhang).

https://doi.org/10.1016/j.optlastec.2026.115643
Received 24 February 2026; Received in revised form 18 May 2026; Accepted 28 May 2026
Available online 30 May 2026
0030-3992/© 2026 Published by Elsevier Ltd.

when an ultra-stable reference is unavailable or inconvenient, single-laser delayed self-interference methods provide a more practical route for narrow linewidth characterization.

According to the length of the fiber delay line (FDL), single-laser self-interference methods can be classified into long-delay and short-delay schemes. In long-delay schemes, the delay time is much longer than the laser coherence time, so the measured spectrum can be approximated by a Lorentzian profile and the linewidth can be directly estimated from the electrical spectrum analyzer (ESA), typically using the −20 dB spectral width. Delayed self-homodyne interferometry[11] is a representative method of this type, but its beat signal is located near zero frequency and is therefore sensitive to low-frequency environmental noise. To overcome this problem, Okoshi *et al.*[12] proposed delayed self-heterodyne interferometry (DSHI), in which an acousto-optic modulator (AOM) is used to shift the beat signal away from the low-frequency region. However, the DSHI method also requires long delay fibers for measuring narrow linewidths. This introduces substantial 1/f noise, which broadens the measured spectrum and leads to a significant overestimation of the laser intrinsic linewidth.

Short-delay FDL schemes can reduce environmental broadening induced by long fibers, but the measured self-heterodyne spectrum no longer follows a simple Lorentzian profile. Instead, it exhibits a coherent envelope, and more sophisticated post-processing is required. Wang *et al.*[9] estimated the linewidth using the power difference between the maximum and minimum of the first-order sidelobe and the frequency separation between the zeroth-order minimum and the center frequency. Zhao *et al.*[13] further derived an analytical equation based on the amplitude difference between adjacent extrema of the coherent envelope. These envelope-based methods enable linewidth measurements at the hundreds-of-hertz level. However, their accuracy depends strongly on the FDL length and the selection of extrema, and the extracted extrema are easily affected by measurement noise.

In addition to envelope-based short-delay DSHI methods, the frequency-noise power spectral density (FN-PSD) method combined with the β-separation line has also been used for sub-kHz intrinsic linewidth measurement[14]. The β-separation line distinguishes frequency-noise components that mainly contribute to central linewidth broadening from those mainly affecting the spectral wings, thereby enabling linewidth estimation from the FN-PSD[15]. This method is particularly useful for separating low-frequency 1/f technical noise from intrinsic white frequency noise. In DSHI measurements, however, the beat-note spectrum is modulated by the delay-interferometer transfer function and does not directly represent the laser FN-PSD. Envelope-ratio-based FN-PSD reconstruction can therefore be combined with the β-separation line to improve the physical consistency of linewidth estimation[16]. Despite its ability to provide physical insight into the noise origin of linewidth broadening, FN-PSD-based linewidth estimation still relies on frequency-noise reconstruction and the selection of an appropriate analysis bandwidth. In contrast, the measured self-heterodyne spectral profile is the most directly accessible observable in DSHI experiments. Extracting linewidth information directly from the measured line shape therefore provides a more intuitive route for practical linewidth characterization, where Voigt profile fitting can be used to separate Lorentzian and Gaussian broadening contributions.

The Voigt profile fitting method was initially applied in fields such as stellar atmosphere research, atomic and plasma spectroscopy[17,18]. Due to its capability to approximate Voigt profiles for any combination of Lorentzian and Gaussian contributions[19], it has been utilized for narrow laser linewidth measurements at the sub-kilohertz level in recent years[20,21]. Compared to the −20 dB spectral width estimation method, this technique can directly extract the Lorentzian component from the measured spectrum, improve the linewidth measurement accuracy from the kilohertz level to hundreds of hertz [22]. Moreover, the algorithm itself is immune to the adverse effects of 1/f noise induced by long-delay fibers [23]. Zheng *et. al.*[24] employed the Voigt method in DSHI to determine a 60 Hz linewidth. However, this method requires the −20 dB linewidth of the measured spectrum as the initial value for iterative calculations. The selection of this initial value is highly sensitive to the fluctuations in the measured spectral lines[13], resulting in significant fluctuations in the calculated working linewidth [25]. This limitation severely restricts the application of the Voigt profile fitting method in linewidth characterization of UNLL, but no systematic analysis or solution to this issue has been proposed to date.

In this work, we propose Mutation Particle Swarm Optimization-Voigt (MPSO-Voigt), to optimize the Voigt spectral iterative procedure for linewidth calculation. In contrast to the traditional Voigt method, which determines the linewidth through stepwise iteration, MPSO-Voigt performs parallel iterative search using a particle swarm, incorporates the analytical relationships among Lorentzian, Gaussian, and Voigt linewidth into the iteration, and introduces a mutation factor together with a dynamic inertia-weight strategy to prevent premature convergence to non-global optimal solutions. We experimentally investigated the fluctuation characteristics of the measured spectrum. Based on these observations, we conducted both numerical simulations and experimental studies on linewidth estimation from noisy self-heterodyne spectrum (SHS). Compared with the traditional Voigt-based approach, MPSO-Voigt can mitigate spectral fluctuations to a large extent, resulting in more accurate linewidth estimates. It also reduces the sensitivity of the measurement to instrument settings and parameter choices, thereby easing the practical requirements on the measurement system. Furthermore, the linewidth results obtained by MPSO-Voigt are consistent with those obtained using the envelope-ratio-based FN-PSD method combined with the β-separation line, confirming the reliability of the proposed method.

2. Principles

2.1. Origin of noise and its suppression strategy

In DSHI measurements using a long FDL, the obtained SHS can be approximated by a Voigt profile, which is the convolution of a Lorentzian component associated with white frequency noise and an approximate Gaussian component induced by 1/f noise[26]. Fig. 1 schematically illustrates an ideal Voigt spectrum obtained by convolving a Lorentzian component with a linewidth of 100 Hz and a Gaussian component with a linewidth of 3250 Hz.

In practical measurements, however,the measured spectrum is inevitably affected by various factors, including ASE noise caused by spontaneous emission, low intermediate frequency intensity noise caused by power fluctuation of pump source and thermal effect in gain

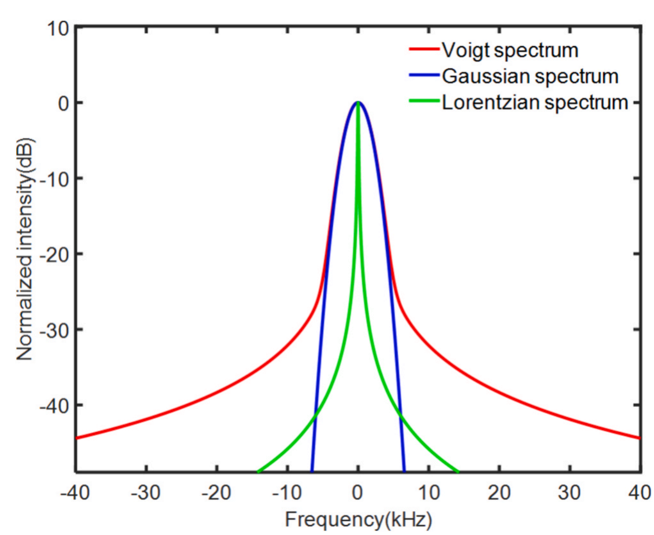

Fig. 1. Simulated spectrum: Lorentzian, Gaussian, and Voigt.

medium, and shot noise caused by optical quantum fluctuations[27–29]. Among them, ASE noise determines the laser signal-to-noise ratio. In order to meet the requirements of the Voigt fitting method, the background noise intensity of the beat spectrum affected by ASE noise is at least −20 dB lower than the intensity of the center frequency of the beat signal. Shot noise, also referred to as quantum noise, arises because light energy propagates as discrete photons. Its emission and detection processes obey random statistical laws, which trigger random fluctuations in light intensity and generate background white noise over the full spectral range. In the observation frequency band of the beat spectrum, we can detect the spectral line fluctuation caused by shot noise from the center frequency to the background noise of the beat spectrum, and the shot noise in other frequency bands will be submerged by ASE noise. In short, the spectral line fluctuation caused by shot noise makes it difficult to accurately obtain the initial linewidth value required by Voigt fitting method.

Two commonly used approaches to obtain a smoother spectral profile are increasing the measurement duration or applying sliding averaging. Increasing the measurement duration extends the integration time (IT), thus suppressing the noise fluctuation caused by statistical uncertainty. However, long measurement time will accumulate low-frequency technical noise[30] such as environmental vibration, which may lead to spectral line distortion. In practical linewidth measurement, moving average is more commonly used. In the electrical spectrum analyzers (ESA), this smoothing is implemented by setting the video bandwidth (VBW), which acts as a low-pass filter on the detected power trace and is mathematically equivalent to a sliding average along the frequency axis. Reducing the VBW efficiently suppresses short-term spectral fluctuations and yields a visually smoother line shape and more stable linewidth readout. At the same time, because the real spectrum is convolved with the instrument response by the VBW filter, an excessively small VBW inevitably causes artificial broadening and distortion of the measured linewidth[31].

Overall, the spectral line fluctuations caused by shot noise in SHS cannot be completely suppressed by smoothing and increasing IT. To facilitate the subsequent numerical simulation experiments, the spectral line fluctuations in the SHS are simplified by superimposing Gaussian white noise generated within a specified range onto the original spectral profile. In addition, the reasonableness of this Gaussian white noise superposition approach will be demonstrated in the experimental section of this paper. As shown in Fig. 2, the fluctuation of any point relative to the original spectral line is controlled within a specified range to simulate the SHS obtained by the instrument under different IT and VBW settings. In numerical experiments, noise fluctuations of 0 dB to 1 dB relative to the original spectral line will be superimposed on the ideal SHS.

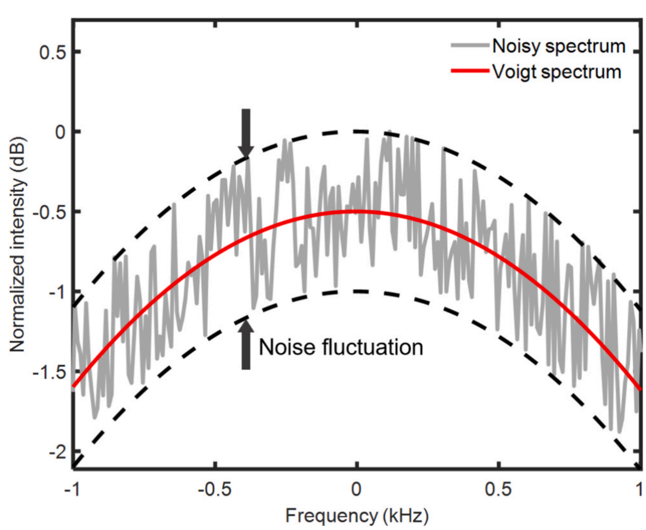

Fig. 2. Numerical simulation SHS with noise.

2.2. Traditional Voigt method

The computational procedure of Voigt is as follows: First, the initial Lorentzian linewidth, $\Delta\nu_L$, is obtained by dividing the −20 dB width of the measured SHS profile, $M(\nu)$, by $2\sqrt{99}$. The −3 dB width of $M(\nu)$ is used as the initial −3 dB width of the Voigt profile, denoted as $\Delta\nu_V$, and the corresponding initial Voigt profile is represented by $V(\nu)$.

Subsequently, the initial Gaussian linewidth, $\Delta\nu_G$, is computed from Eq.(1)[32]. The Lorentzian and Gaussian line shapes, generated from $\Delta\nu_L$ and $\Delta\nu_G$ according to Eq.(2) and Eq.(3), are convolved to produce a Voigt profile. This generated $V(\nu)$ is compared with the −20 dB width of $M(\nu)$. If the discrepancy is significant, $\Delta\nu_V$ is updated based on the new Voigt profile, $V'(\nu)$, and the entire process is repeated iteratively until the −20 dB width of the generated $V'(\nu)$ converges with that of the $M(\nu)$. The traditional Voigt flowchart is shown in Fig. 3.

$$\Delta\nu_V = \frac{1}{2}\left(1.0692\Delta\nu_L + \sqrt{0.866639\Delta\nu_L^2 + 4\Delta\nu_G^2}\right) \tag{1}$$

Where $\Delta\nu_V$ is the −3 dB width of the Voigt profile, $\Delta\nu_L$ and $\Delta\nu_G$ are the Lorentzian and Gaussian linewidths, respectively, and L denotes the normalized Lorentzian line shape centered at $\nu = \nu_0$, given by the following expression:

$$L(\nu) = \frac{1}{2\pi}\frac{1}{(\nu-\nu_0)^2/\Delta\nu_L + \Delta\nu_L/4} \tag{2}$$

Correspondingly, G is the normalized Gaussian line shape centered at $\nu = \nu_0$, defined as:

$$G(\nu) = \frac{2}{\Delta\nu_G\sqrt{\pi/\text{In}2}}\exp\left(-4\text{In}2(\nu-\nu_0)^2/\Delta{\nu_G}^2\right) \tag{3}$$

It should be noted that the core of the traditional Voigt method lies in

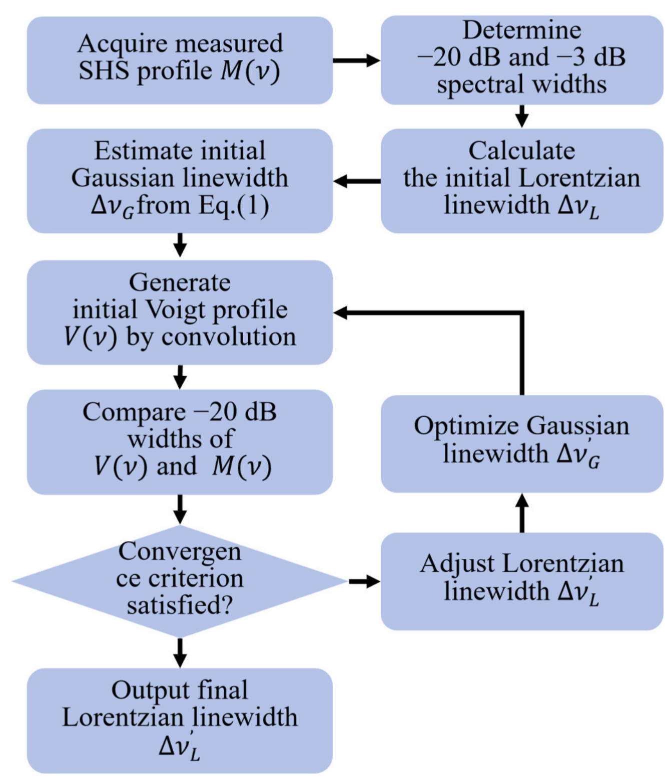

Fig. 3. Voigt process flowchart.

using the −20 dB width of the measured SHS profile as the primary basis for the initial estimation of the Lorentzian linewidth. This initial solution not only determines the construction of the initial Voigt profile, but also further affects the final linewidth decomposition results. However, as described in section 2.1, the spectral fluctuations in the SHS caused by shot noise cannot be completely eliminated through smoothing processing and increasing the IT, which consequently affects the linewidth calculation results of the traditional Voigt method.

For clarity and reproducibility, all symbols and variables used in this section are summarized in Table 1.

2.3. MPSO optimized Voigt iteration

To address the issue that the accuracy of the traditional Voigt method is highly sensitive to the choice of initial values, MPSO algorithm is employed to optimize the iterative Voigt profile fitting process, as detailed in Fig. 4. It should be emphasized that, when evaluating the Gaussian linewidth $\Delta\nu'_G$, the analytical relationship among the Lorentzian, Gaussian, and Voigt linewidths is introduced. This approach reduces the optimization targets in the PSO-Voigt procedure from two independent parameters, namely the Lorentzian linewidth $\Delta\nu'_L$ and the Gaussian linewidth $\Delta\nu'_G$, to a single parameter $\Delta\nu'_L$, thereby lowering the search scope and overall computational cost of the PSO algorithm. Additionally, this method physically constrains the relationship between the Lorentzian, Gaussian, and Voigt linewidths, which improves the reliability of the converged results while simultaneously reducing the search space of the PSO algorithm.

Furthermore, by introducing a mutation operator and a dynamically adjusted inertia weight, as indicated by the blue modules in Fig. 4, the MPSO-Voigt algorithm is developed based on the PSO-Voigt. This modification effectively reduces the risk of premature convergence to a non-global optimum during the iterative process[33]. The implementation of MPSO-Voigt is as follows:

Table 1
List of symbols and descriptions.

Symbol	Description	Symbol	Description
$\Delta\nu_V$	−3 dB linewidth of the Voigt spectral profile	$P(i)'_{pos}$	Updated particle position
$\Delta\nu_{V\text{-}20\,dB}$	−20 dB linewidth of the Voigt spectral profile	$P(i)_{pb}$	Personal best position
$\Delta\nu_L$	−3 dB linewidth of the Lorentzian spectral profile	$P(i)_{gb}$	Global best position
$\Delta\nu_G$	−3 dB linewidth of the Gaussian spectral profile	m	Predefined population size
$\Delta\nu_{m\text{-}3dB}$	−3 dB linewidth of the measured SHS profile	w	Inertia weight
$\Delta\nu_{m\text{-}20\,dB}$	−20 dB linewidth of the measured SHS profile	w_{max}	Maximum inertia weight
$L(\nu)$	Normalized Lorentzian line shape	w_{min}	Minimum inertia weight
$G(\nu)$	Normalized Gaussian line shape	$iter$	current iteration index
$V(\nu)$	Voigt spectral profile generated by convolution of $L(\nu)$ and $G(\nu)$	$iter_{max}$	maximum number of iterations
$M(\nu)$	Measured SHS profile	c_1	Individual learning factor
ν	Frequency variable	c_2	Social learning factor
ν_0	Center frequency of the spectral line	r_1, r_2, r_3	Independent random variables uniformly distributed over [1]
i	Particle index	m_R	Predefined mutation factor
$P_\nu(i)$	Current particle velocity	b_1	Lower boundary value of the particles
$P'_\nu(i)$	Updated particle velocity	b_2	Upper boundary value of the particles
$P(i)_{pos}$	Current particle position		

$$P(i)'_\nu = w^*P(i)_\nu + c_1{}^*r_1{}^*\left(P(i)_{pb} - P(i)_{pos}\right) + c_2{}^*r_2{}^*\left(P(i)_{gb} - P(i)_{pos}\right) \tag{4}$$

Where $P'_\nu(i)$ denotes the updated particle velocity, $P_\nu(i)$ is the current particle velocity, and $P_{pos}(i)$ is the current particle position, with $i \in \{1, \cdots, m\}$ being the particle index and m is the predefined population size. The parameter w represents the inertia weight. The individual and social learning factors are denoted by c_1 and, respectively, while r_1 and r_2 are random numbers uniformly distributed in the interval [1]. The personal best position and the global best position are represented by $P(i)_{pb}$ and $P(i)_{gb}$, respectively. The particle position is updated as follows:

$$P(i)'_{pos} = P(i)_{pos} + P(i)'_\nu \tag{5}$$

where $P(i)'_{pos}$ denotes the updated particle position. To ensure that the particles remain within the defined boundaries, the following operation is applied:

$$P(i)'_{pos} = \text{Max}\left(\text{Min}\left(P(i)'_{pos}, b_2\right), b_1\right) \tag{6}$$

where b_1 and b_2 represent the lower and upper boundary values of the particles, respectively. When the random numbers r_1 and r_2 are both less than the predefined mutation factor m_R, a mutation operation is applied to the updated particle position $P(i)'_{pos}$ as follows:

$$P(i)'_{pos} = b_1 + (b_2 - b_1)^*r_3 \tag{7}$$

where r_3 is a random number uniformly distributed in the range [1]. After applying Eq.(4) to Eq.(7), this process yields the updated particle positions and velocities. The inertia weight w is updated using the classical linear variation strategy:

$$w = w_{max} - (w_{max} - w_{min})\frac{iter}{iter_{max}} \tag{8}$$

where $w_{\max}$ and $w_{\min}$ denote the maximum and minimum inertia weights, respectively. Here, iter is the current iteration index, and iter_{max} is the maximum number of iterations.

In the traditional Voigt method, the discrepancy between the.

−20 dB widths of $V\prime(\nu)$ and $M(\nu)$ is used as the error function[28], which essentially discards all spectral profile information above the −20 dB level. In contrast, this paper employs the Mean Squared Error (MSE) between $V\prime(\nu)$ and $M(\nu)$ as the error function to improve the accuracy of the linewidth calculation. The MSE is calculated as follows:

$$MSE = \frac{1}{N}\sum_{\nu_{left}}^{\nu_{right}}\left(V\prime(\nu) - M(\nu)\right)^2 \tag{9}$$

where $\nu \in [\nu_{left}, \nu_{right}]$ defines the spectral range above the −20 dB level, and N denotes the total number of data points in the profile.

The parameter configuration of the MPSO-Voigt algorithm includes the population size, the initial particle velocities, the cognitive and social learning factors, the inertia weight, the mutation factor, the maximum number of iterations, and the convergence threshold. The specific settings are as follows:

Based on the measured spectrum $M(\nu)$, the −3 dB width $\Delta\nu_{m\text{-}3dB}$ and the −20 dB width $\Delta\nu_{m\text{-}20dB}$ are used in (1) to construct the initial Lorentzian spectrum $L(\nu)$ and the initial Gaussian spectrum $G(\nu)$. Their convolution yields the initial Voigt spectrum $V(\nu)$. The −20 dB width of $V(\nu)$, denoted $\Delta\nu_{V\text{-}20dB}$, is then calculated and divided by $2\sqrt{99}$ to obtain the initial estimate of the laser linewidth $\Delta\nu_L$, which is much larger than the theoretical intrinsic linewidth of the laser. This initial linewidth $\Delta\nu_L$ is taken as the upper bound of the particle search range, while the lower bound is set to 1 Hz. This search interval has a significant impact on the convergence speed and search direction of the PSO optimization process [34]. The population size m is set to 50, which lies within the empirical

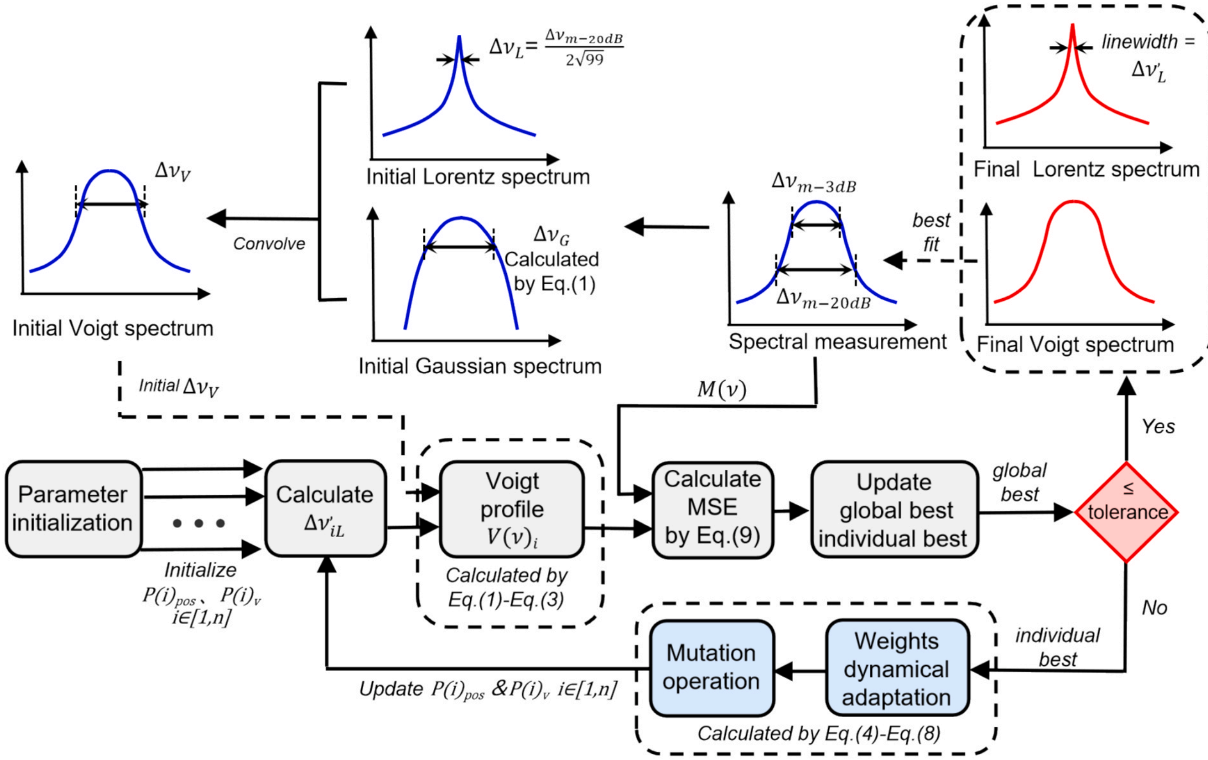

Fig. 4. MPSO-Voigt process flowchart.

range of 20–50 and provides a compromise among population diversity, the balance between exploration and exploitation, and computational cost, so that the algorithm maintains good convergence performance and efficiency for most optimization problems [35]. The initial particle velocity $P_\nu(i)$ is set to 15% of the total search range, which falls within the commonly used interval of 10%–20%. This setting avoids excessively large velocities that cause particles to overshoot the optimum and excessively small velocities that trap them in local minima, thereby balancing the exploration and exploitation capabilities of the algorithm [36] . The cognitive and social learning factors are chosen as $c_1 = 1.6$ and $c_2 = 2$, corresponding to a fully informed particle swarm configuration with both c_1 and c_2 nonzero, so that both convergence speed and global search performance are maintained [37]. The maximum and minimum inertia weights are set to $w_{\max} = 0.9$ and $w_{\min} = 0.4$, respectively. A relatively large inertia weight in the early iterations accelerates the contraction of the search space, whereas the gradually reduced inertia weight in the later iterations facilitates fine local search and high-accuracy solutions[38]. The mutation factor m_R is set to 0.3, and by randomly resetting the positions of a small fraction of particles after each iteration, the global exploration capability of the algorithm is enhanced[35].

According to Eq.(4) to Eq.(7), the inertia weight and mutation operation are dynamically adjusted, and the particle positions and velocities are initialized to solve for the Lorentzian linewidth $\Delta\nu_L'$ associated with each particle. The obtained $\Delta\nu_L'$ together with the initial $\Delta\nu_{V\text{-}3dB}$ are then substituted into Eq.(1) to compute the updated Gaussian linewidth $\Delta\nu_G'$, and Eq.(2) and Eq.(3) are used to generate the next Voigt spectrum $V'(\nu)$. Based on Eq.(8), the error function is evaluated to determine the fitness of each particle, and the personal best and global best values are updated accordingly. This procedure is iterated until the global best value falls below the predefined convergence threshold, at which point the corresponding $\Delta\nu_L'$ is taken as the final estimate of the laser linewidth.

3. Simulation and Comparison

In numerical experiments, noise fluctuations of 0 dB to 1 dB relative to the original spectral line will be superimposed on the ideal SHS. In this case, the effective linewidth estimation performance of Voigt fitting method, PSO-Voigt, and MPSO-Voigt will be systematically compared.

See Fig. 5 shows the results processed by the traditional Voigt algorithm with different levels of noise added across the entire spectrum. As observed, in the absence of noise, the Voigt profile calculated by the traditional Voigt fits the simulated SHS perfectly, yielding a laser linewidth of 98 Hz, which is very close to the preset simulated value. However, as the noise level increases, the calculated Voigt profile gradually deviates from the simulated SHS contour, and the deviation of the obtained laser linewidth from the preset value becomes larger.

Notably, when the added noise level is only 0.5 dB, the error already reaches 84 Hz by the traditional Voigt. The results processed by the PSO-Voigt algorithm are shown in Fig. 6. When the added noise level is 0.5 dB, the error is only 16 Hz by the PSO-Voigt. Although the calculated linewidth value also increases with the noise level, the computational error is significantly reduced compared to the traditional Voigt method. Fig. 7 presents the results processed by the MPSO-Voigt algorithm, whose calculated linewidth values are similar to those obtained by the PSO-Voigt algorithm.

To more intuitively observe the advantages of mutation operation for MPSO-Voigt, Fig. 8 compares the iterative behaviors of the three methods at a noise level of 1 dB. Since the initial linewidth is taken from the −20 dB linewidth widened by noise, the traditional Voigt method converges to an excessive value. Although the PSO-Voigt approach reduces the dependence on the initial value, it may still be trapped in a local optimum. The estimated linewidth stagnates near 153 Hz from the seventh iteration onward. In contrast, MPSO-Voigt benefits from mutation operations and dynamic weight adjustment, converges rapidly to approximately 150 Hz by the second iteration, escapes the local optimum at the sixteenth iteration, and subsequently reaches the convergence criterion to complete the estimation.

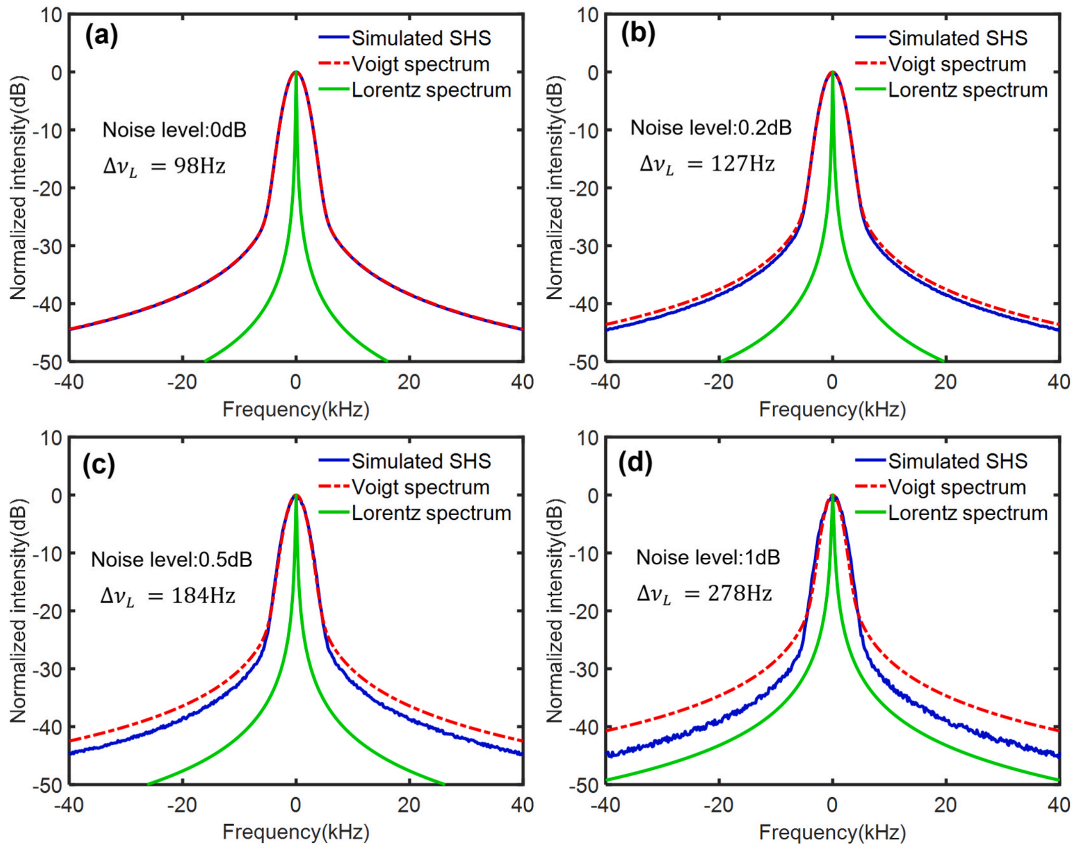

Fig. 5. Linewidth $\Delta\nu_L$ measured by the traditional Voigt method. (a) 0 dB, (b) 0.2 dB, (c) 0.5 dB, (d) 1 dB.

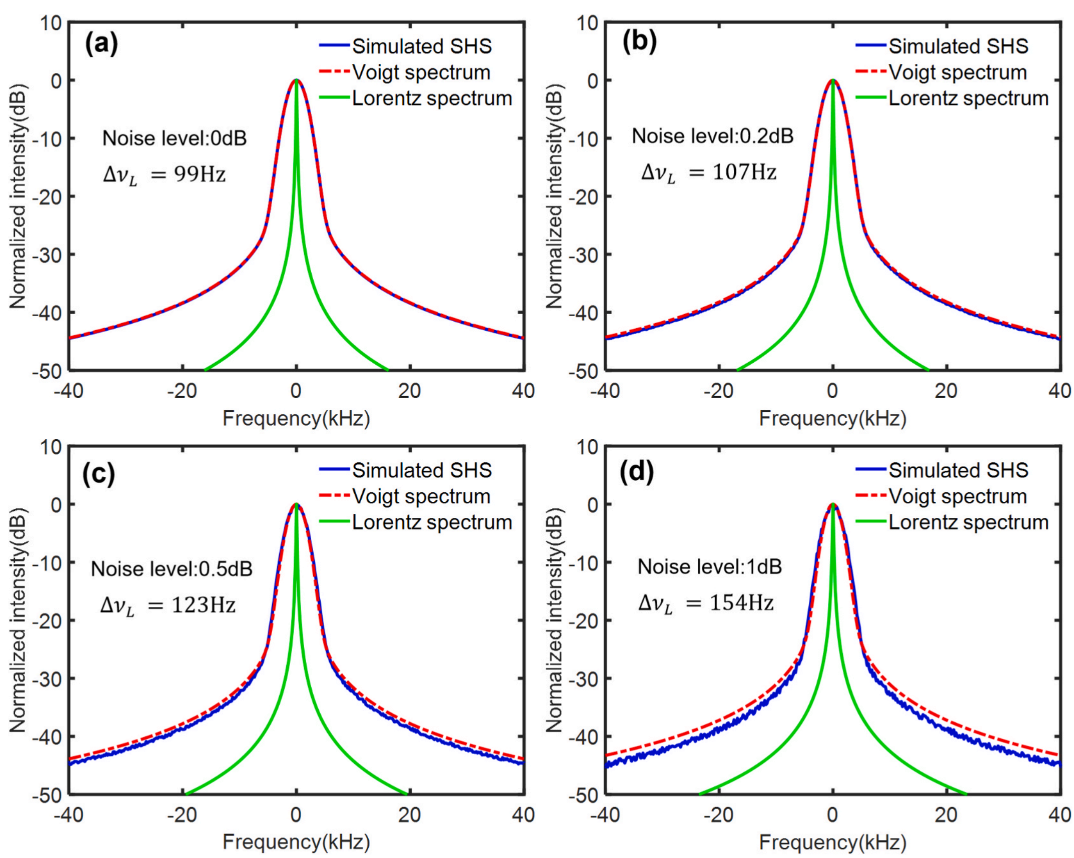

Fig. 6. Linewidth $\Delta\nu_L$ measured by the the PSO-Voigt method. (a) 0 dB, (b) 0.2 dB, (c) 0.5 dB, (d) 1 dB.

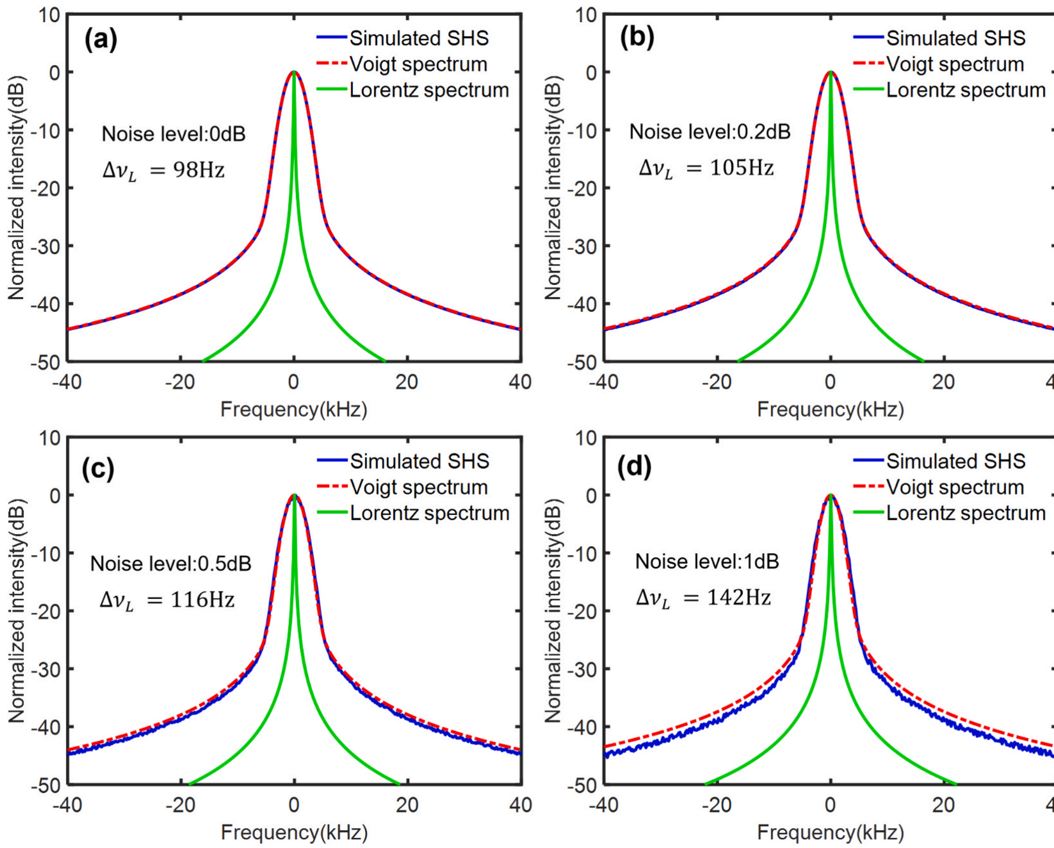

Fig. 7. Linewidth $\Delta\nu_L$ measured by the MPSO-Voigt method. (a) 0 dB, (b) 0.2 dB, (c) 0.5 dB, (d) 1 dB.

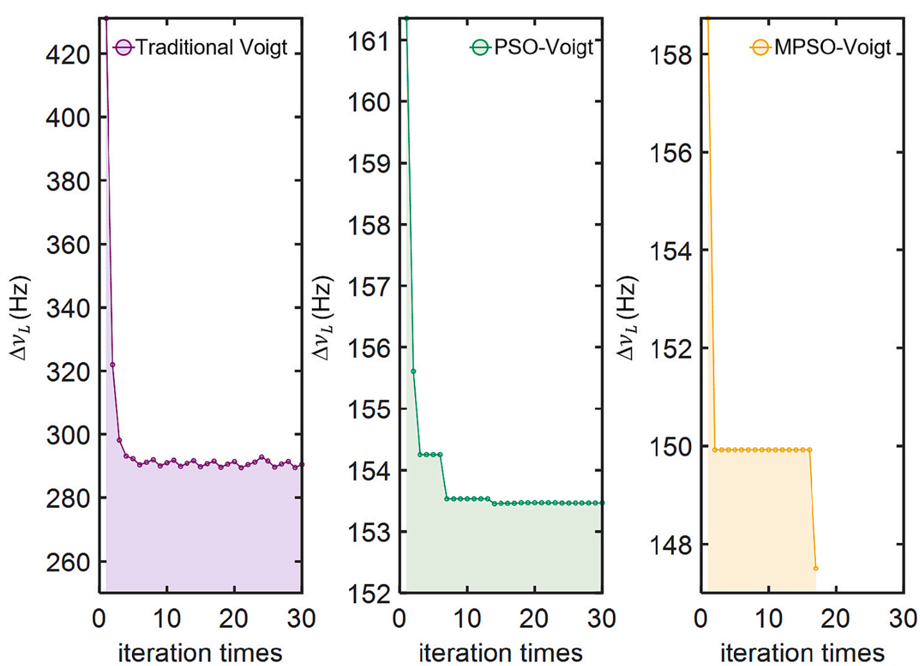

Fig. 8. Comparison of iterative processes of traditional Voigt, PSO-Voigt, and MPSO-Voigt methods.

In order to more intuitively compare the influence of $M(\nu)$ on the results obtained by the three methods, Monte Carlo analysis is performed on each noise level to calculate the fluctuation range of linewidth value, as shown in Fig. 9. Compared with the traditional Voigt, the maximum fluctuations of PSO-Voigt and MPSO-Voigt are lower. It is worth noting that the fluctuation of the proposed MPSO-Voigt results is slightly lower than that of the PSO-Voigt results,because the mutation operation allows it to escape from local optima and achieve convergence.

Compared with the traditional Voigt method, in the presence of 1 dB relative noise in SHS, the measurement error is reduced from 178% to 42% and the measurement fluctuation is decreased from 47% to 7%.

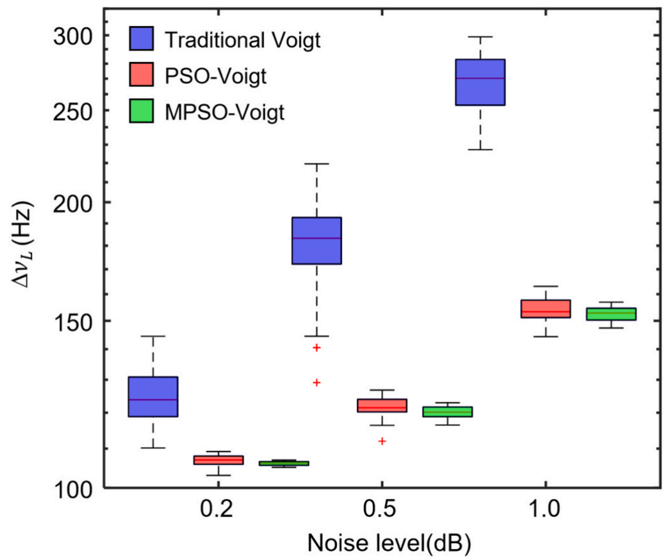

Fig. 9. Comparison of calculated $\Delta\nu_L$ using traditional Voigt, PSO-Voigt, and MPSO-Voigt methods under different noise levels.

These results clearly demonstrate that the proposed MPSO-Voigt method significantly improves the stability and accuracy of linewidth measurement in comparison with the traditional Voigt-based approach.

4. Experiment and analysis

4.1. Experimental setup

As shown in Fig. 10, the experimental setup adopts a DSHI configuration. The laser output first passes through an optical isolator (ISO) and is then split by a 10:90 fiber coupler. The optical power launched into the linewidth measurement system was 9.8 mW, corresponding to approximately 10 dBm. The 10% branch is frequency-shifted by 40 MHz using an acousto-optic modulator (AOM) driven by a 10 MHz signal generator, while the 90% branch is launched into a 100 km fiber delay line (FDL). After propagation through the FDL, the output optical power of this arm is approximately −10.46 dBm. The two beams are recombined by a 2 × 2 coupler and then injected into a balanced photodetector (BPD).

Since the optical power after the FDL may still exceed the linear operating range of the BPD, additional optical attenuators are inserted before the detector to adjust the optical powers of the two input arms. The optical power entering each single-ended output port of the 2 × 2 coupler is kept below −20 dBm to avoid detector saturation and ensure that the BPD operates within its linear response range. The generated beat signal is acquired by an oscilloscope (OSC), and the SHS is obtained through power spectral density (PSD) calculation. With a 12-bit ADC architecture, the OSC samples at 500 Msps and supports an acquisition time of 1–300 ms to capture SHS under different integration times (ITs). Based on Zhao *et al.*[13] regarding delay fiber length effect on DSHI spectral profiles, a 100 km fiber delay is selected for subsequent linewidth measurements, ensuring the measured SHS is well approximated by a Voigt profile under combined white and shot noise.

In addition, ESA-based DSHI measurement is a more commonly used and standard approach for laser linewidth characterization. This is mainly because an ESA provides high spectral measurement sensitivity and dynamic range, and can obtain stable spectral traces through appropriate RBW/VBW settings.

In comparison, an OSC was selected in this work because it can provide sufficient measurement performance for the present experiments. Moreover, compared with an ESA, an OSC is a more commonly used and indispensable instrument in most laboratory environments. It can also display the original time-domain beat signal in real time, which helps verify the beat-signal quality, optimize the measurement system, and reduce the influence of time-domain signal distortion on linewidth extraction. To evaluate whether the OSC-based acquisition scheme meets the linewidth measurement requirements of this work, the next subsection compares the results obtained using the ESA and OSC-based schemes.

4.2. Comparison of measurement results obtained using different Instruments

To verify whether the OSC-based acquisition and post-processing meet the linewidth measurement requirements, we compared the SHS obtained using an ESA and an OSC for the same fiber laser under a 100-km-fiber-delay DSHI configuration. The acquisition and processing schemes are listed in Table 2.

As shown in Fig. 11, the SHS profiles obtained by the ESA and OSC show good agreement, both before and after 2 kHz moving-average processing. In particular, no obvious difference is observed near the spectral center or in the region used for −20 dB width extraction. This indicates that, under the present experimental conditions, OSC acquisition and post-processing do not introduce obvious additional spectral broadening or profile distortion compared with ESA measurement.

It should be noted that the moving average used in OSC post-processing is functionally similar to VBW smoothing in ESA measurements. Both can suppress random spectral fluctuations, but improper smoothing may broaden the spectral envelope and affect linewidth extraction. Therefore, the smoothing parameter should be carefully selected to balance noise suppression and spectral-shape preservation. In this work, the smoothing parameter was determined based on spectral

Table 2
Data sources and processing methods.

Label	Data source and processing	Key parameters
OSC result	Processed from data acquired by OSC	FR of SHS = 3.72 Hz
ESA result	Processed from data acquired by ESA	FR of SHS = 3.67 Hz
OSC, 2 kHz avg.	Moving average of “OSC result”	SAW = 2 kHz
ESA, 2 kHz avg.	Moving average of “ESA result”	SAW = 2 kHz

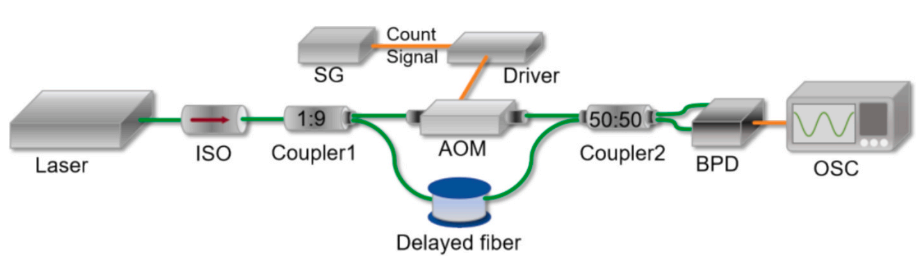

Fig. 10. DSHI Measurement Setup.

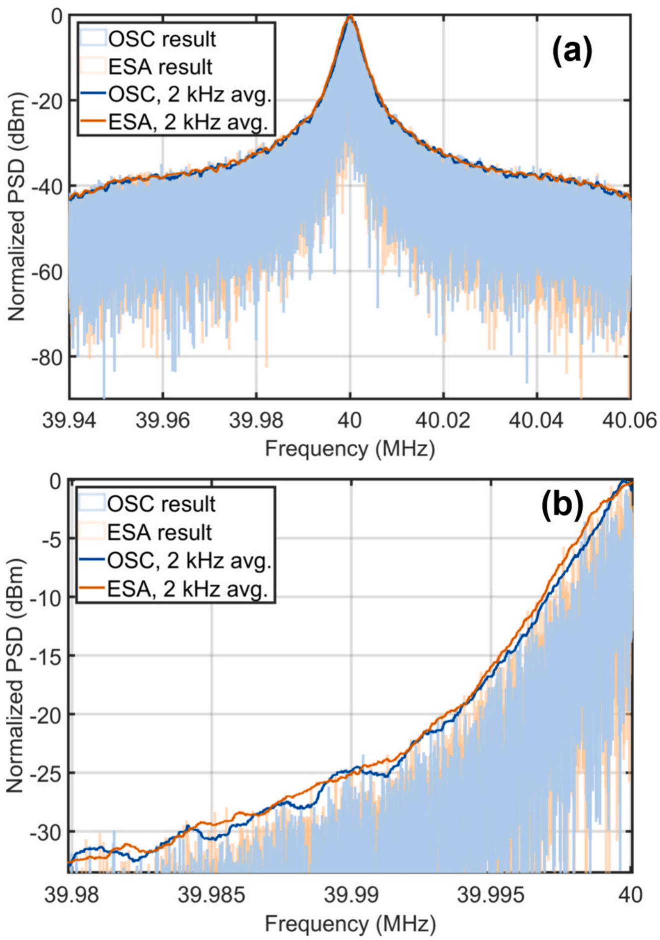

Fig. 11. (a) Comparison of SHS results from different acquisition methods (b) Local magnification of the SHS in (a).

fluctuations and the metric introduced later, rather than being chosen arbitrarily.

Overall, the ESA and OSC-based results are highly consistent under the same DSHI conditions. Therefore, the OSC scheme satisfies the linewidth extraction requirements and is suitable for studying the effects of integration time, smoothing parameters, and spectral fluctuations on Voigt linewidth decomposition.

4.3. Spectral line fluctuation analysis

As shown in Fig. 10, we obtain the SHS of a semiconductor laser based on the DSHI.

See Fig. 12(a) shows that the OSC noise is much lower than the background noise of the SHS. The background noise envelope of the SHS remains at a nearly constant level, which arises from the influence of ASE noise. From Fig. 12(b), it can be observed that the spectral line of the SHS is submerged by ASE noise at −60 dB, which is far below the −20 dB spectral line required for the Voigt method-based measurement. We perform sliding averaging processing on the SHS with a 2 kHz window, and extract the fluctuation level of the SHS at a digital sliding average window (SAW) of 2 kHz and an IT of 0.3 s by subtracting the smoothed SHS from the original one, as illustrated in Fig. 12(c). We further calculate its histogram distribution, corresponding to the blue bars in Fig. 12(d). The simulated white Gaussian noise has an amplitude range matched to that of the beat signal; its PSD is derived using the SHS algorithm, with the corresponding PSD histogram plotted as the green line in Fig. 12(d). It can be observed that the histogram distribution of the SHS is similar to that of white Gaussian noise, both exhibiting skewed distributions. This not only verifies that shot noise is white noise acting on the entire spectral line, but also demonstrates that in numerical experiments, assuming Gaussian white noise for SHS spectral line fluctuations can approximate the real situation.

Matching with the VBW, we introduce SAW to perform sliding averaging on the SHS obtained by processing the beat frequency signal obtained by OSC. Here, we conducted comparative experiments on different IT and SAW to further elucidate their effects on SHS spectral line fluctuations.

As shown in Fig. 13 and Fig. 14, the center frequency of the spectrum at 40 MHz is mapped to 0 Hz. When the SAW is fixed at 4 kHz, the overall shape of the SHS in Fig. 13(a) and its local details in Fig. 13(b) change significantly with the IT. As shown in Fig. 14(a), varying the SAW barely affects the spectral profile. However, the magnified view in Fig. 14(b) shows the spectral line rises with increasing SAW. A larger SAW is mainly adopted to yield smoother SHS. To quantitatively characterize the local fluctuations of the spectral profile, the standard deviation of the sliding standard deviation (SDSSD) is introduced as a metric to evaluate the local average fluctuation level of the SHS. A smaller SDSSD indicates weaker local fluctuations and thus a smoother line shape.

As shown in Fig. 15(a), the SDSSD reaches a minimum with increasing SAW, implying that a larger SAW is not necessarily better. Instead, the appropriate SAW value is closely related to the measurement duration, and there exists a relatively optimal range. Once the SAW exceeds this range, the SHS exhibits pronounced broadening and line-shape distortion, making it unsuitable for linewidth estimation.It can also be observed from Fig. 15(b) that the influence of measurement duration on SDSSD is not linear. There is a turning point in the measurement duration, beyond which further extension of the duration leads to a saturated or even weakened improvement in the smoothing effect. These results indicate that merely adjusting the SAW and the measurement duration can mitigate, but not eliminate, the impact of noise on linewidth estimation. Under the present parameter settings, the minimum SDSSD is approximately 0.1 dB.

4.4. Linewidth measurement experiment

The measurement setup is identical to that shown in Fig. 10, and the DSHI method is employed to measure the linewidths of both a semiconductor laser(LXNLM-1550-L03-T10-FA) and a fiber laser(NKT E15). For each self-heterodyne spectral measurement, the IT was fixed at 0.3 s to ensure sufficient spectral resolution. The SAW parameter was appropriately adjusted to minimize the SDSSD. A comparative linewidth measurement across different types of lasers was conducted to evaluate the applicability of the proposed method. The key parameters of this semiconductor laser and fiber laser provided by the manufacturer are shown in Table 3. It can be seen that the phase noise at 100 Hz in semiconductor lasers is much higher than that in fiber lasers, which reflects that the effective linewidth of semiconductor lasers is expected to be larger than that of fiber lasers. The comparative experiment is therefore designed to confirm this linewidth ordering and to test whether the proposed method can reliably distinguish these two regimes.

The linewidth measurement results for the fiber laser are presented in Fig. 16. The Lorentzian fitting curves, with their respective linewidths determined by the widths of the spectral line at −20 dB and −3 dB, are presented in Fig. 16(a).

It can be observed that neither of these two Lorentzian spectral lines can fit the SHS. Meanwhile, the results indicate that when the laser linewidth is estimated using the −3 dB width of the SHS, the obtained linewidth is 1.39 kHz. When estimated using the −20 dB width of the SHS, the obtained laser linewidth is 714 Hz. The −20 dB measurement approach does suppress the broadening effect caused by 1/f frequency noise to some extent, and it is more accurate than the −3 dB width measurement since the influence of 1/f noise is less pronounced away from the center frequency. Nevertheless, the −20 dB width

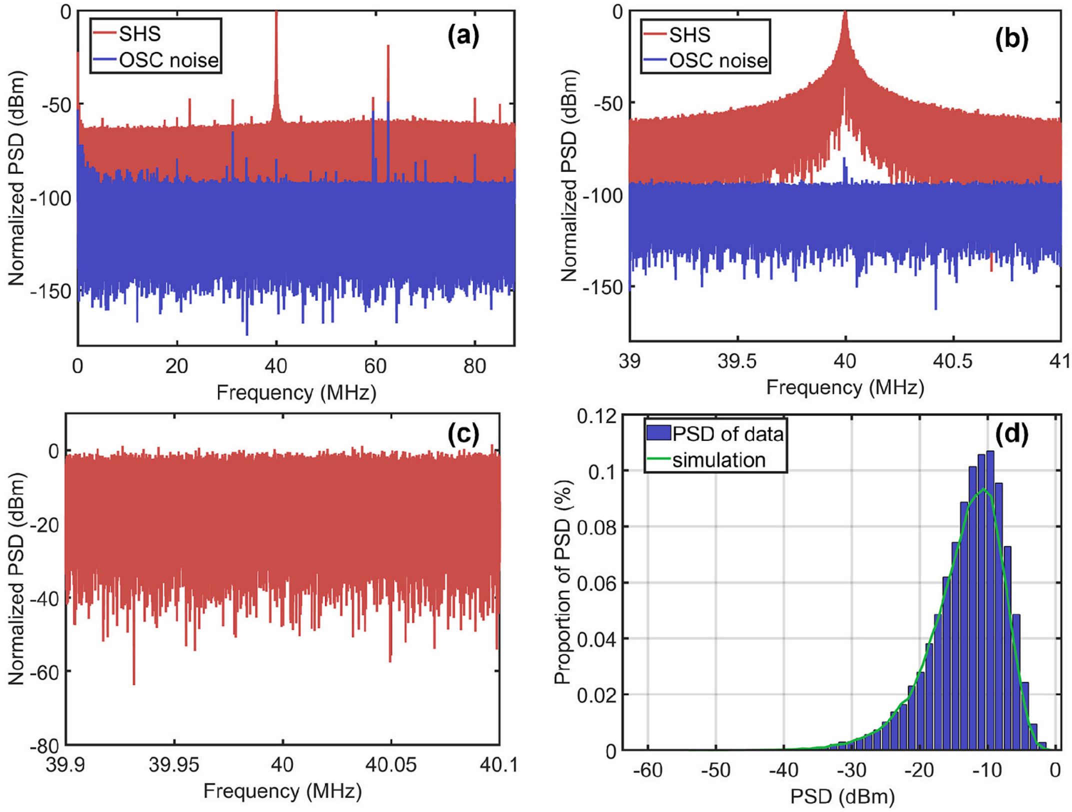

Fig. 12. (a) SHS obtained from semiconductor laser.(b) Local Magnification of the SHS in (a). (c) The fluctuation result after subtracting the SHS moving average.(d) Histograms of SHS and Gaussian white noise PSD.

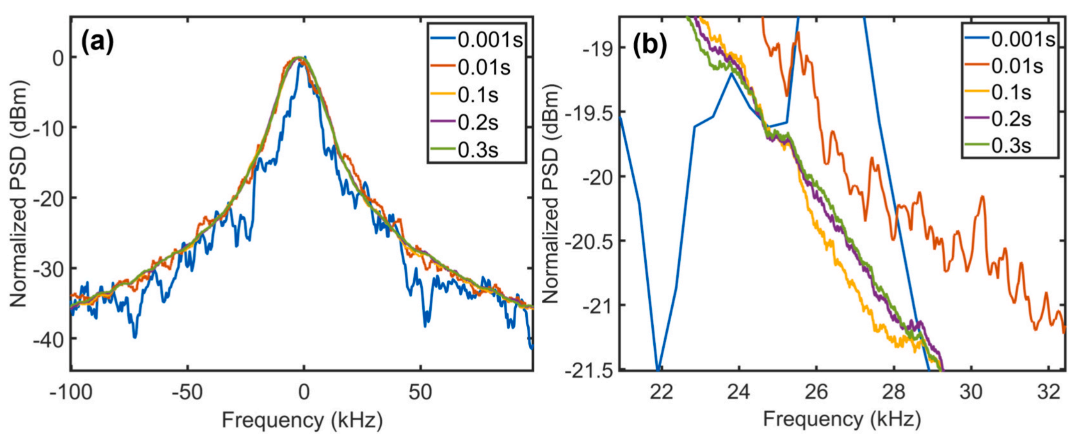

Fig. 13. (a) SHS for different IT with SAW = 4 kHz. (b) Local magnification of the SHS in (a).

measurement still significantly overestimates the intrinsic linewidth of the ultra-narrow linewidth fiber laser, as the Lorentzian component is much smaller than the Gaussian component. Fig. 16(b) shows the Voigt spectral line obtained by fitting with the traditional Voigt method, as well as the separated Lorentzian and Gaussian spectral lines. It can be observed that the part above −20 dB of the Voigt spectral line fitted by the traditional Voigt method almost overlaps with the original self-heterodyne difference spectrum. However, the linewidth corresponding to the separated Lorentzian spectral line is 298 Hz, which is much higher than the intrinsic linewidth value provided by the manufacturer. The reason for the increased measured linewidth is as mentioned earlier: high-noise or ambiguously defined data points in the measured spectrum will directly interfere with the accuracy of initial value selection, and this interference is particularly significant in 100 Hz-level UNLLs, leading to a substantial increase in calculation errors. Fig. 16 (c) and 16 (d) show the Voigt spectral lines fitted by the PSO-Voigt method and MPSO-Voigt method, respectively; their parts above −20 dB also almost overlap with the original SHS, and the linewidths corresponding to their separated Lorentzian spectral lines are 213 Hz and 201 Hz, respectively.

The linewidth measurement results for the semiconductor laser are presented in Fig. 17. The results indicate that the linewidth of the semiconductor laser estimated from the −20 dB spectral width is 2.53 kHz, which is substantially larger than the corresponding value of 714 Hz for the fiber laser. Using the MPSO-Voigt method, the extracted linewidth is 1.05 kHz, which is also higher than the linewidth of 201 Hz obtained for the fiber laser. Both values are significantly larger than the intrinsic linewidths specified by the manufacturer, and this outcome is consistent with the differences in the specifications listed in Table 3.

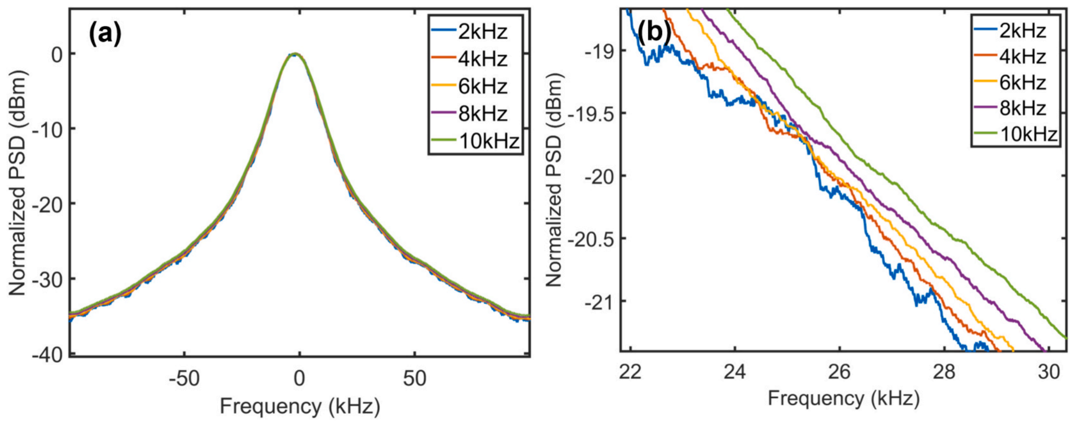

Fig. 14. (a) SHS for different SAW values with an IT of 0.3 s. (b) Local magnification of the SHS in (a).

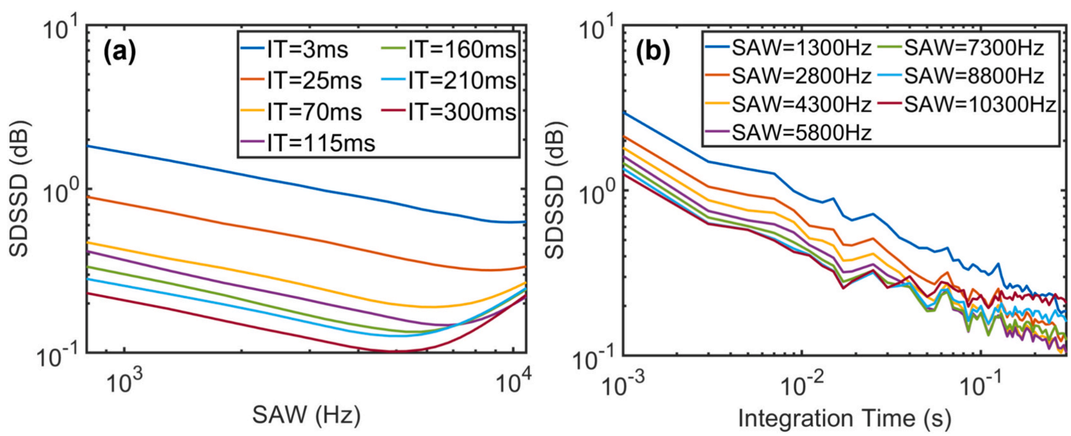

Fig. 15. (a)Variation of SDSSD with SAW for different IT.(b)Variation of SDSSD with IT for different SAW.

Table 3
Parameters of the two lasers.

Laser	Intrinsic linewidth(Hz)	Phase noise ($(\mathrm{Rad}/\sqrt{\mathrm{Hz}})/\mathrm{m}$ (@100 Hz)	Frequency instability (MHz) (within 1 h)
LXNLM-1550-L03-T10-FA	<100	−108	50
NKT E15	<100	−127	20

From a physical perspective, a single-frequency fiber laser typically features a longer resonant cavity and a longer intracavity photon lifetime. This leads to lower phase noise than that of a single-frequency semiconductor laser [39], which manifests in the frequency domain as a narrower integrated linewidth. In addition, single-frequency fiber lasers generally exhibit better frequency stability, which likewise implies reduced phase noise.

This does not indicate a failure of the linewidth measurement methodology. Rather, it demonstrates that the proposed MPSO-Voigt approach can reliably estimate the linewidths of different types of UNLLs. These results suggest that, when characterizing UNLLs, particularly for applications in which frequency stability is critical, one should not judge performance solely based on the intrinsic linewidth determined by the resonator. Instead, attention should be paid to the Lorentzian component within the integrated linewidth, as it more faithfully represents the effective linewidth of the laser over the measurement duration. This further highlights the importance of accurately and robustly isolating the Lorentzian contribution from the measured spectrum.

In addition, to further demonstrate the better stability of the proposed MPSO-Voigt method for measuring linewidth, Fig. 18 summarizes the results of 20 repeated linewidth measurements performed on the fiber laser. The linewidth separated by the MPSO-Voigt method ranges from 190 Hz to 213 Hz, while that separated by the PSO-Voigt method ranges from 198 Hz to 240 Hz. Due to occasional premature convergence, the result distribution of the PSO-Voigt method is less concentrated than that of the MPSO-Voigt method. The linewidth separated by the traditional Voigt method ranges from 265 Hz to 354 Hz. It can be observed that the proposed MPSO-Voigt method in this work exhibits better stability and is closer to the theoretical intrinsic linewidth of the laser, with the measurement fluctuation of the calculated linewidth reduced by 75% compared with the conventional Voigt method.

4.5. Comparison of measurement results obtained using different Instruments

In traditional Lorentzian fitting, previous studies have indicated that the influence of 1/f noise induced broadening becomes weaker as the analyzed SHS region moves farther away from the spectral center. However, the practical influence of the fitting range on linewidth extraction has not been systematically examined, making the selection of an appropriate fitting range ambiguous. To address this issue, a fitting-range sensitivity analysis was performed on the same measured SHS data using both Lorentzian fitting and the proposed MPSO-Voigt method.

Specifically, the SHS widths at −10 dB, −20 dB, −30 dB, and −40 dB were used as the fitting targets for Lorentzian fitting, as shown in Fig. 19.

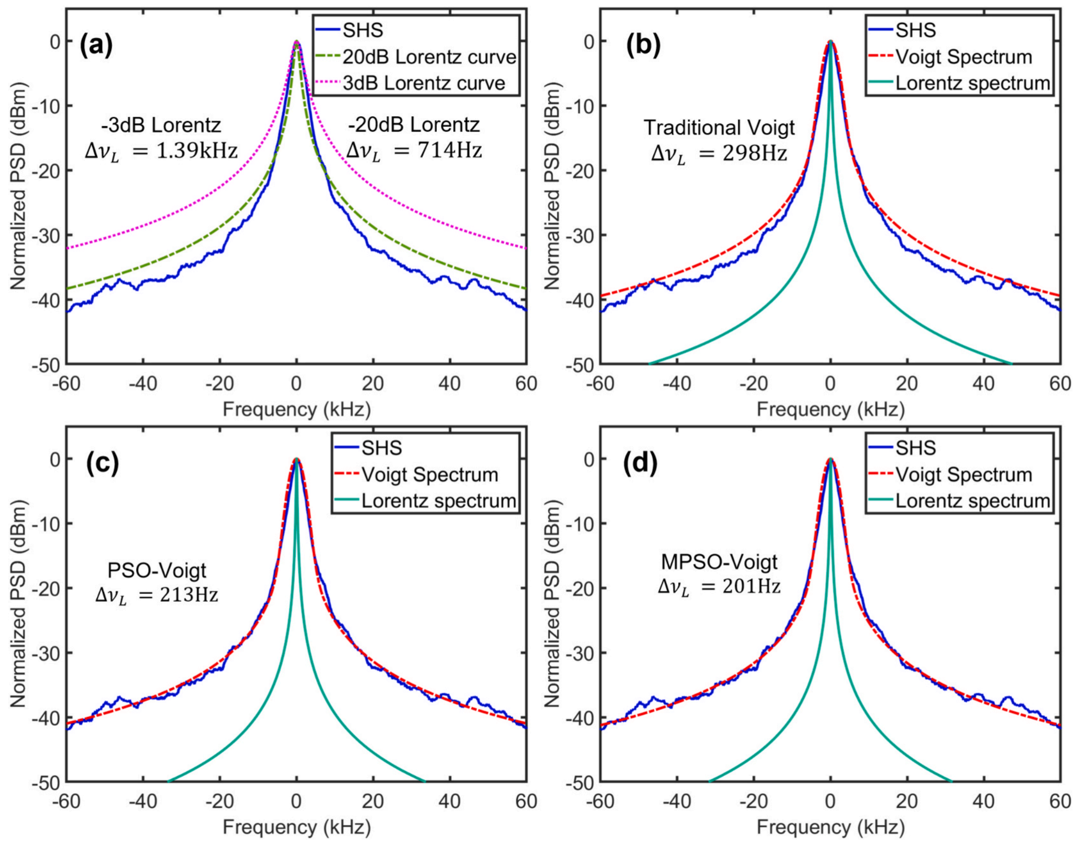

Fig. 16. Linewidth measurement results of fiber laser.(a) −20 dB and −3dB estimation methods. (b) Traditional Voigt; (c) PSO-Voigt; (d) MPSO-Voigt.

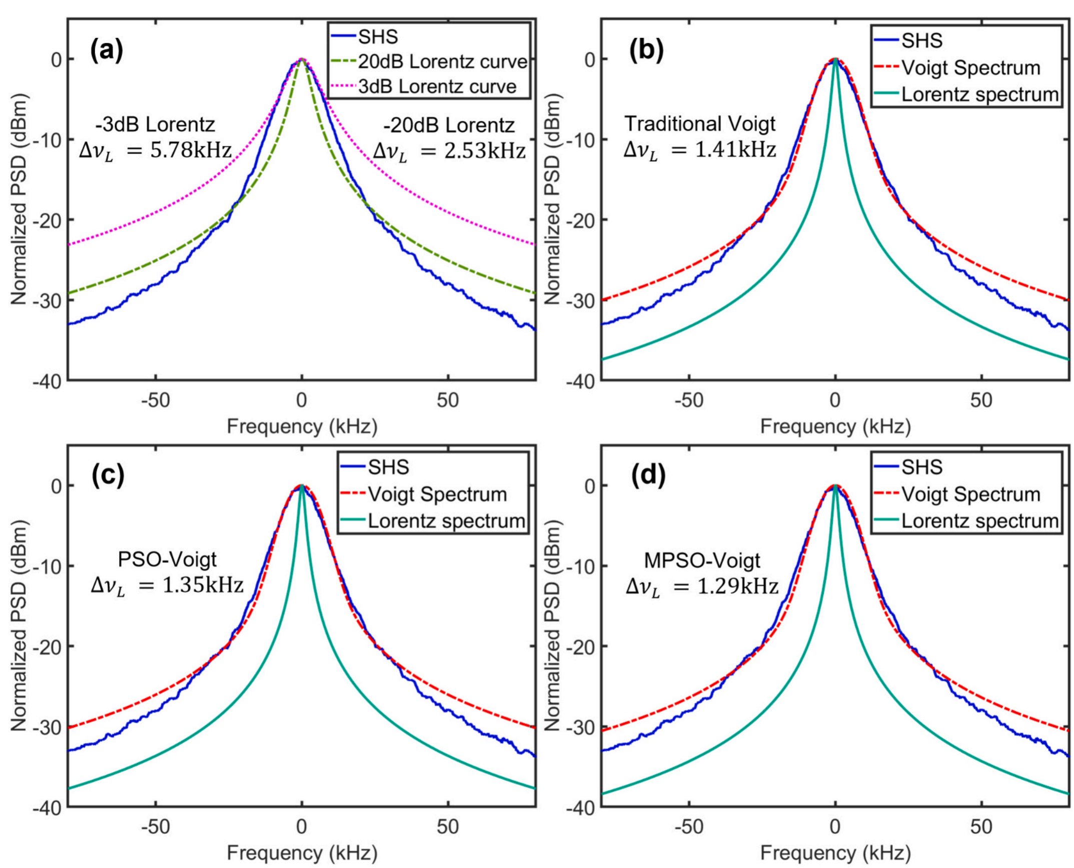

Fig. 17. Linewidth measurement results of semiconductor laser.(a) −20 dB and −3 dB estimation methods. (b) Traditional Voigt; (c) PSO-Voigt; (d) MPSO-Voigt.

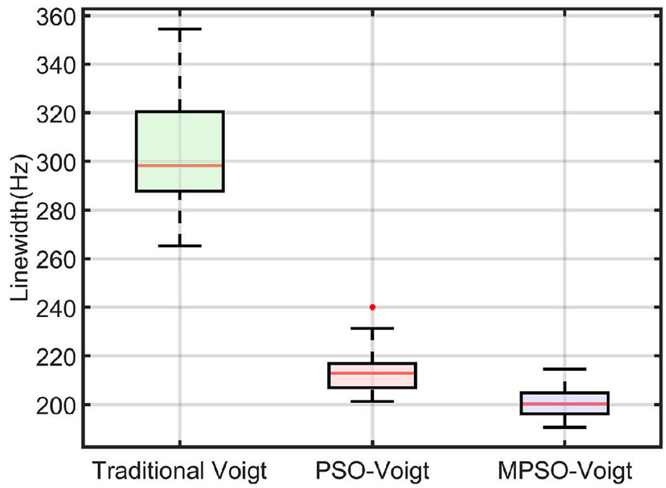

Fig. 18. Comparison of linewidth estimation results among the three methods.

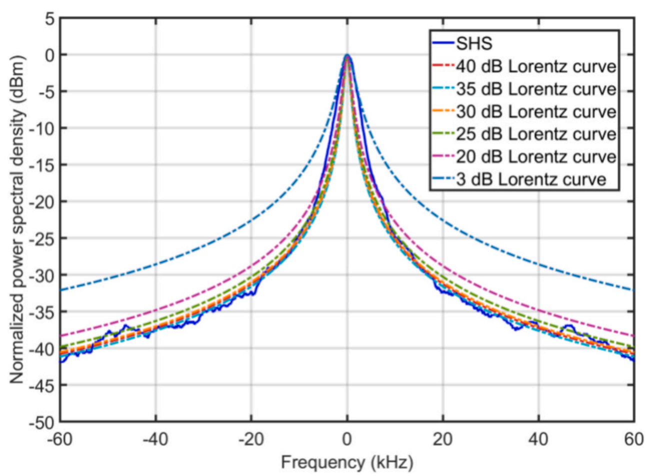

Fig. 19. Lorentzian fitting results under different target SHS widths.

As the fitting target moves farther away from the spectral center, the extracted Lorentzian linewidth gradually decreases. This is because, compared with the −3 dB width, the SHS width at a lower power threshold is less affected by Gaussian broadening induced by 1/f noise, leading to a smaller Lorentzian linewidth estimate.

However, this variation is not linear. As the fitting target is further extended toward the far spectral tail, the decrease in linewidth becomes progressively weaker and eventually tends to saturate. Meanwhile, the signal-to-noise ratio in the far-tail region decreases, and local spectral fluctuations become more pronounced, thereby increasing the uncertainty of linewidth estimation. Therefore, when the lower fitting threshold is below −20 dB, the Lorentzian fitting results exhibit certain fluctuations.

Correspondingly, the spectral regions above −20 dB, −30 dB, and −40 dB were further used as the fitting ranges for the MPSO-Voigt method. Fig. 20 compares the Lorentzian fitting results obtained with different target SHS widths and the results obtained using MPSO-Voigt. Compared with Lorentzian fitting, which relies only on the SHS width at a specific power threshold, MPSO-Voigt uses the overall SHS profile information within the selected fitting range and extracts the Lorentzian component through Voigt decomposition. Therefore, it provides a more stable Lorentzian linewidth estimate. Nevertheless, when fluctuations in the far spectral tail significantly distort the spectral shape, the uncertainty of linewidth extraction by MPSO-Voigt also increases.

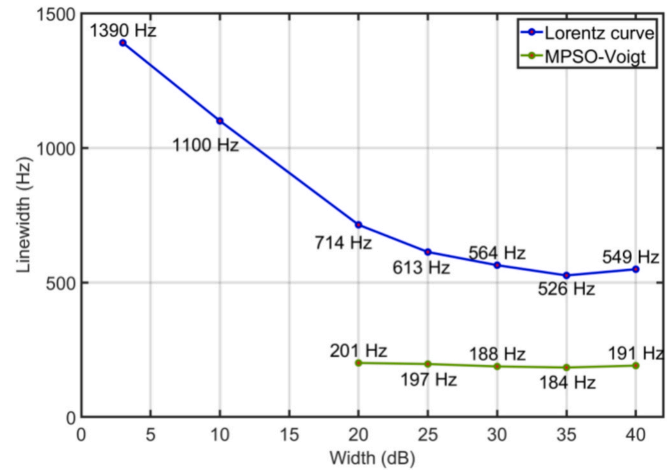

Fig. 20. Comparison of linewidth results obtained using Lorentzian fitting with different target SHS widths and the MPSO-Voigt method.

4.6. Linewidth validation using the FN-PSD/β-separation line method

For comparison, the linewidth of the fiber laser was estimated using the FN-PSD method combined with the β-separation line, with the FN-PSD reconstructed by the DSHI envelope-ratio method. The reconstructed FN-PSD with β-separation line are shown in Fig. 21(a), and the linewidth results obtained under different lower integration limits are

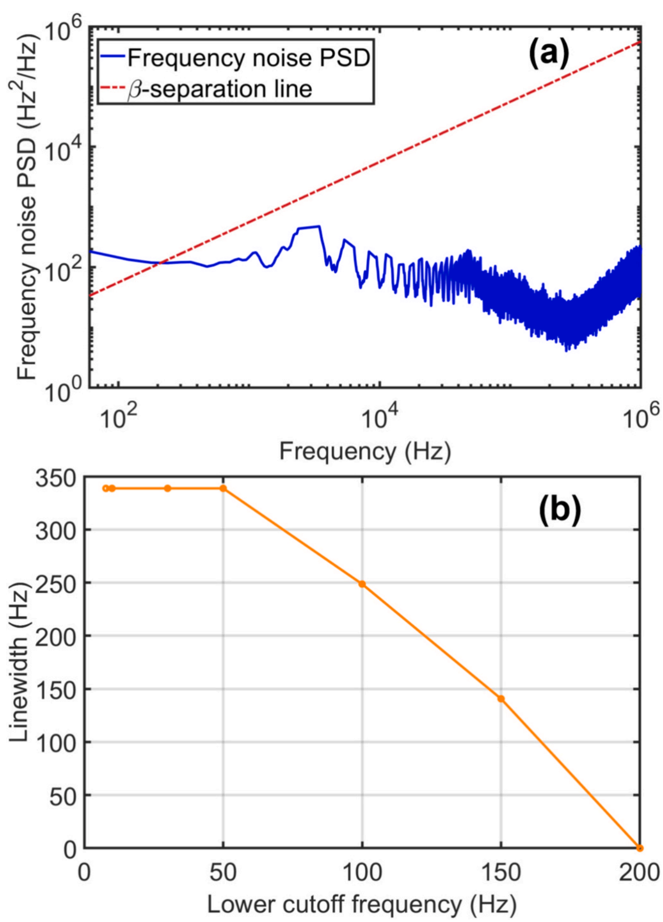

Fig. 21. Linewidth estimation based on FN-PSD with β-separation line analysis. (a) FN-PSD with β-separation line. (b) Estimated linewidths with different lower integration limits.

presented in Fig. 21(b). When the lower integration limit was set to 3 Hz, 10 Hz, 30 Hz, and 50 Hz, the estimated linewidth remained approximately 330 Hz. When the lower limit was increased to 100 Hz, the linewidth decreased to 248 Hz, and it approached zero at 200 Hz. This indicates that lower integration limits include more low-frequency technical-noise contributions, such as slow drift, vibration, thermal perturbation, and residual feedback noise. Although increasing the lower integration limit can suppress these contributions, the estimated linewidth should be interpreted as an effective value within the selected frequency range rather than a full-band linewidth including all low-frequency noise. Therefore, to reduce the influence of technical noise and to remain consistent with the cutoff frequency used in related DSHI envelope-ratio experiments[16], 100–150 Hz was selected as the lower integration limit range for the β-separation line analysis. Under this condition, the linewidth results are consistent with those obtained using the MPSO-Voigt method.

It is also important to emphasize that the nominal linewidth specified by the manufacturer usually refers to the intrinsic linewidth determined by the laser structure. When such a value is obtained using experimental methods such as DSHI, it is generally further specified as an integrated linewidth or operating linewidth. The linewidth extracted in this work is the effective Lorentzian linewidth obtained from the measured SHS through Voigt decomposition. Therefore, it is not strictly equivalent to the intrinsic linewidth, but is closer in meaning to the integrated or operating linewidth.

Under the room-temperature and atmospheric-pressure conditions used in this work, low-frequency technical noise induced by environmental perturbations, mechanical vibration, and temperature fluctuation can broaden the Lorentzian linewidth[40], making the measured effective linewidth higher than the nominal intrinsic linewidth. Meanwhile, the results obtained from the FN-PSD with β-separation line analysis also confirm that low-frequency technical noise makes a significant contribution to effective-linewidth broadening.

Overall, the significance of narrow-linewidth measurement lies not only in obtaining a linewidth value, but also in accurately characterizing the frequency stability of a laser under practical operating conditions and revealing its deviation from the theoretical design value, thereby providing more useful guidance for laser design, fabrication, and application optimization.

5. Discussion

The results indicate that the main limitation of conventional Voigt fitting in ultra-narrow linewidth measurement lies in its sensitivity to the initial fitting values and to spectral fluctuations in the self-heterodyne spectrum. In the proposed MPSO-Voigt method, the fitting process is reformulated as a constrained global search problem. The analytical relations among the Lorentzian, Gaussian, and Voigt linewidths are used to restrict the parameter space, while mutation factors and dynamic inertia weights are introduced to reduce the risk of premature convergence. Both simulations and experiments confirm this trend: compared with conventional Voigt fitting, the MPSO-Voigt method produces smaller linewidth errors and lower result fluctuations, particularly when the SHS is affected by noise-induced spectral fluctuations.

It should be noted that, for lasers with relatively broad intrinsic linewidths, where the Lorentzian component dominates the measured SHS, traditional Lorentzian fitting based estimation methods are generally sufficient under appropriate measurement conditions and do not necessarily require complex post-processing algorithms. In contrast, for 100-Hz-level UNLLs, the Lorentzian component in the measured SHS is relatively weak and can be easily masked by Gaussian broadening and spectral fluctuations. In this case, more sophisticated post-processing methods are needed to reliably obtain the effective linewidth, such as the proposed MPSO-Voigt method for robust Voigt-profile decomposition, or the FN-PSD method combined with the β-separation line based on DSHI envelope reconstruction for linewidth estimation in the frequency-noise domain.

In addition, the observed spectral fluctuations in the SHS are analyzed, and the simulation and experimental results show that these fluctuations are consistent with a white-noise mechanism.The results further show that integration time and smoothing affect linewidth extraction by changing the level of spectral fluctuation and the shape of the spectral envelope. Longer integration time and moderate smoothing reduce random fluctuations, whereas excessive smoothing distorts the Voigt profile and biases the fitted linewidth. The proposed SDSSD metric provides a quantitative basis for balancing noise suppression and spectral distortion during parameter selection. Finally, the experimental results obtained using the MPSO-Voigt method are consistent with the linewidth measurement results obtained using the FN-PSD with β-separation line method. Overall, this study provides a robust fitting algorithm and offers practical guidance for selecting measurement and post-processing parameters.

However, the current work can be further optimized in the following two respects. First, the spectral model is restricted to Voigt profiles shaped by a combination of white and flicker noise, summarized by a single fluctuation metric. In situations where the laser exhibits more complex frequency-noise spectra, non-Voigt line shapes or strongly time-varying technical noise, the current formulation may not be sufficient. A logical next step is therefore to extend the MPSO-Voigt algorithm to incorporate more general line-shape models and to combine linewidth estimation with direct frequency-noise PSD measurements. This would allow a more detailed decomposition of the measured linewidth into underlying physical noise processes and enable cross-validation against alternative techniques such as short-delay self-heterodyne and unbalanced interferometric methods. Second, the experimental validation is limited to representative semiconductor and fiber lasers. These already cover distinct linewidth regimes and demonstrate that the proposed method can discriminate between them, but they do not span the full diversity of practical laser architectures and operating conditions. Future work should include a broader set of devices, for example different cavity designs, different wavelength bands and lasers operating under deliberate perturbations such as current or temperature modulation. Such studies would help to delineate the range of validity of the MPSO-Voigt approach and to refine the recommended measurement and smoothing strategies for different classes of lasers.

6. Conclusion

This study proposes MPSO-Voigt, which replaces the critical iterative steps in Voigt profile fitting with a MPSO process and incorporates the relational constraints among Lorentzian, Gaussian, and Voigt linewidths. The measured average effective linewidth is 97 Hz lower than that of the traditional Voigt method, and the fluctuation of the linewidth measurement results is reduced by approximately 40%. In addition, the linewidth results obtained using the FN-PSD method combined with the β-separation line criterion are consistent with those obtained using MPSO-Voigt, further supporting the reliability of the proposed method. It overcomes the constraints of initial value dependence and noise sensitivity associated with the traditional Voigt method, and provides a high-performance solution for the accurate linewidth measurement of UNLLs.

Author statement.

We declare that this manuscript is original, has not been published before and is not currently being considered for publication elsewhere.

We confirm that the manuscript has been read and approved by all named authors and that there are no other persons who satisfied the criteria for authorship but are not listed.

We further confirm that the order of authors listed in the manuscript has been approved by all of us. We understand that the Corresponding Author is the sole contact for the Editorial process. He is responsible for communicating with the other authors about progress, submissions of revisions and final approval of proofs.

Funding.

This work was supported by National Natural Science Foundation of China (NSFC) under Grant (62175100), and Fundamental Research Funds for the Central Universities (2024300447).

Data underlying the results presented in this paper are not publicly available at this time but maybe obtained from the authors upon reasonable request.

CRediT authorship contribution statement

Hongren Li: Writing – original draft, Visualization, Validation, Supervision, Software, Methodology, Data curation, Conceptualization. **Ningmu Zou:** Writing – review & editing, Supervision, Resources. **Tian Xiao:** Validation, Software, Investigation, Data curation. **Nasheeta Mazhar:** Visualization, Validation, Investigation. **Yixin Zhang:** Writing – review & editing, Supervision, Methodology, Funding acquisition. **Jiaqi Ma:** Validation, Formal analysis. **Xinyu Wang:** Software, Investigation, Formal analysis. **Xuping Zhang:** Supervision, Funding acquisition. **Erming Liang:** Validation, Investigation.

Declaration of competing interest

The authors declare that they have no known competing financial interests or personal relationships that could have appeared to influence the work reported in this paper.

Data availability

Data will be made available on request.

References

[1] K. Schuh, F. Buchali, W. Idler, T.A. Eriksson, L. Schmalen, W. Templ, L. Altenhain, U. Dümler, R. Schmid, M. Möller, K. Engenhardt, Single carrier 1.2 Tbit/s transmission over 300 km with PM-64, in: QAM at 100 GBaud, in: 2017 Optical Fiber Communications Conference and Exhibition (OFC), 2017, pp. 1–3.

[2] C. Di Fronzo, N.A. Holland, A.L. Mitchell, S.J. Cooper, M. Valentini, D. Martynov, L. Prokhorov, C.M. Mow-Lowry, Laser frequency stabilization with the use of homodyne quadrature interferometers, Class. Quantum Grav. 41 (2024) 065010, https://doi.org/10.1088/1361-6382/ad13c4.

[3] L. Dang, D. Huang, Z. Su, Y. Li, F. Li, C + L-band tunable sub-kHz linewidth single frequency fiber laser by combining a fiber sub-ring with a saturable absorber, Opt. Laser Technol. 181 (2025) 111944, https://doi.org/10.1016/j.optlastec.2024.111944.

[4] W. Zhang, L. Stern, D. Carlson, D. Bopp, Z. Newman, S. Kang, J. Kitching, S. B. Papp, Ultranarrow Linewidth Photonic-Atomic Laser, Laser Photonics Rev. 14 (2020) 1900293, https://doi.org/10.1002/lpor.201900293.

[5] R. Morita, T. Inoue, M. Yoshida, K. Enoki, M. De Zoysa, K. Ishizaki, S. Noda, Demonstration of high-power photonic-crystal surface-emitting lasers with 1-kHz-class intrinsic linewidths, Optica 11 (2024) 333, https://doi.org/10.1364/OPTICA.505406.

[6] G. Gredat, H. Liu, F. Bretenaker, Thermal phase fluctuations in optically pumped dual-frequency vertical external-cavity surface-emitting lasers for cesium clocks based on coherent population trapping, J. Appl. Phys. 126 (2019) 173104, https://doi.org/10.1063/1.5123444.

[7] J. Gao, K. Jiao, G. Zhao, R. Yin, J. Yang, X. Yan, W. Chen, W. Ma, S. Jia, State Key Laboratory of Quantum Optics and Quantum Optics Devices, Shanxi University, Taiyuan 030006, China, Collaborative Innovation Center of Extreme Optics, Shanxi University, Taiyuan 030006, China, Silesian College of Intelligent Science and Engineering, Yanshan University, Qinhuangdao 066000, China, Research on linewidth narrowing and frequency control technology of quantum cascade lasers based on optical feedback and optical phase-locked loops, Acta Phys. Sin. 74 (2025) 014204. Doi: 10.7498/aps.74.20241414.

[8] T. Liu, Q.J. Wang, Fundamental frequency noise and linewidth broadening caused by intrinsic temperature fluctuations in quantum cascade lasers, Phys. Rev. B 84 (2011) 125322, https://doi.org/10.1103/PhysRevB.84.125322.

[9] Z. Wang, C. Ke, Y. Zhong, C. Xing, H. Wang, K. Yang, S. Cui, D. Liu, Ultra-narrow-linewidth measurement utilizing dual-parameter acquisition through a partially coherent light interference, Opt. Express 28 (2020) 8484, https://doi.org/10.1364/OE.387398.

[10] T. Takakura, K. Iga, T. Tako, Linewidth Measurement of a Single Longitudinal Mode AlGaAs Laser with a Fabry-Perot Interferometer, Jpn. J. Appl. Phys. 19 (1980) L725–L727, https://doi.org/10.1143/JJAP.19.L725.

[11] Z. Liu, H. Zheng, C. Li, Z. Qi, C. Zhang, T. Li, Z. Bai, Advances in Laser Linewidth Measurement Techniques: a Comprehensive Review, Micromachines 16 (2025) 990, https://doi.org/10.3390/mi16090990.

[12] T. Okoshi, K. Kikuchi, A. Nakayama, Novel method for high resolution measurement of laser output spectrum, Electron. Lett. (UK) 16 (1980) 630–631, https://doi.org/10.1049/el:19800437.

[13] Z. Zhao, Z. Bai, D. Jin, Y. Qi, J. Ding, B. Yan, Y. Wang, Z. Lu, R.P. Mildren, Narrow laser-linewidth measurement using short delay self-heterodyne interferometry, Opt. Express 30 (2022) 30600, https://doi.org/10.1364/OE.455028.

[14] C. Zhang, L. Huang, T. Guan, Y. Mao, J. Li, L. Gao, W. Huang, L. Shi, G. Yin, T. Zhu, Dynamic exploration of laser linewidth compression in resonant feedback external-cavity laser, Appl. Phys. Lett. 124 (2024) 191103, https://doi.org/10.1063/5.0193777.

[15] G. Di Domenico, S. Schilt, P. Thomann, Simple approach to the relation between laser frequency noise and laser line shape, Appl. Opt. 49 (2010) 4801, https://doi.org/10.1364/AO.49.004801.

[16] Y. Li, Z. Fu, L. Zhu, J. Fang, H. Zhu, J. Zhong, P. Xu, X. Chen, J. Wang, M. Zhan, Laser frequency noise measurement using an envelope-ratio method based on a delayed self-heterodyne interferometer, Opt. Commun. 435 (2019) 244–250, https://doi.org/10.1016/j.optcom.2018.10.065.

[17] I. Marshall, J. Higinbotham, S. Bruce, A. Freise, Use of voigt lineshape for quantification of *in vivo*[1] H spectra, Magnetic Resonance in Med 37 (1997) 651–657, https://doi.org/10.1002/mrm.1910370504.

[18] W.I.F. David, J.C. Matthewman, Profile refinement of powder diffraction patterns using the Voigt function, J. Appl. Crystallogr. 18 (1985) 461–466, https://doi.org/10.1107/S0021889885010718.

[19] L.B. Mercer, 1/f frequency noise effects on self-heterodyne linewidth measurements, J. Lightwave Technol. 9 (1991) 485–493, https://doi.org/10.1109/50.76663.

[20] M. Ahmadi, T. Dutta, M. Mukherjee, A Scalable Narrow Linewidth High Power Laser for Barium Ion Optical Qubit (2023), https://doi.org/10.48550/ARXIV.2312.03388.

[21] A. Canagasabey, A. Michie, J. Canning, J. Holdsworth, S. Fleming, H.-C. Wang, M. L. Åslund, A Comparison of delayed Self-Heterodyne Interference Measurement of Laser Linewidth using Mach-Zehnder and Michelson Interferometers, Sensors 11 (2011) 9233–9241, https://doi.org/10.3390/s111009233.

[22] T. Tepper García, Voigt profile fitting to quasar absorption lines: an analytic approximation to the Voigt-Hjerting function: A new method to compute Voigt profiles, Monthly Notices of the Royal Astronomical Society 369 (2006) 2025–2035. Doi: 10.1111/j.1365-2966.2006.10450.x.

[23] J.-Y. Ma, X.-H. Zhan, S. Wang, Z.-Q. Yin, W. Chen, G.-C. Guo, Z.-F. Han, Theoretical analysis for estimating laser integrated linewidth via frequency-noise power spectral density, Opt. Lett. 49 (2024) 5893, https://doi.org/10.1364/OL.540021.

[24] Z. Zheng, Q. Luo, X. Wang, X. Ma, W. Zhang, W. Fang, X. Chen, S. Huang, Y. Zhou, W. Gao, Comparison of Different Linewidth measuring Methods for Narrow Linewidth Laser, Sensors 23 (2022) 122, https://doi.org/10.3390/s23010122.

[25] S. Chen, Y. Jia, H. Chen, P. Guo, Q. Xu, L. Wang, Y. Zhang, Approximate Voigt function formula for laser-induced breakdown spectroscopy fitting, Appl. Opt. 60 (2021) 4120, https://doi.org/10.1364/AO.416677.

[26] M. Chen, Z. Meng, J. Wang, W. Chen, Ultra-narrow linewidth measurement based on Voigt profile fitting, Opt. Express 23 (2015) 6803, https://doi.org/10.1364/OE.23.006803.

[27] S.B. Foster, A.E. Tikhomirov, Pump-Noise Contribution to Frequency Noise and Linewidth of Distributed-Feedback Fiber Lasers, IEEE J. Quantum Electron. 46 (2010) 734–741, https://doi.org/10.1109/JQE.2009.2035335.

[28] M. Deroh, E. Lucas, K. Hammani, G. Millot, B. Kibler, Stabilized single-frequency sub-kHz linewidth Brillouin fiber laser cavity operating at 1 μm, Appl. Opt. 62 (2023) 8109, https://doi.org/10.1364/AO.495877.

[29] L. Wu, Z. Ji, W. Ma, D. Su, Y. Zhao, L. Xiao, S. Jia, Narrow laser linewidth measurement with the optimal demodulated Lorentzian spectrum: erratum, Appl. Opt. 63 (2024) 2561, https://doi.org/10.1364/AO.522944.

[30] W. Loh, S. Yegnanarayanan, F. O'Donnell, P.W. Juodawlkis, Ultra-narrow linewidth Brillouin laser with nanokelvin temperature self-referencing, Optica 6 (2019) 152, https://doi.org/10.1364/OPTICA.6.000152.

[31] S.P.Ó. Dúill, L.P. Barry, Simplified Laser Frequency Noise Measurement using the delayed Self-Heterodyne Method, Photonics 11 (2024) 813, https://doi.org/10.3390/photonics11090813.

[32] A.S. AlOmar, Line width at half maximum of the Voigt profile in terms of Gaussian and Lorentzian widths: Normalization, asymptotic expansion, and chebyshev approximation, Optik 203 (2020) 163919, https://doi.org/10.1016/j.ijleo.2019.163919.

[33] Y. Han, F. Zeng, L. Fu, F. Zheng, GA-PSO Algorithm for Microseismic Source Location, Appl. Sci. 15 (2025) 1841, https://doi.org/10.3390/app15041841.

[34] Y. Huang, M. Lu, Y. Hu, Q. Wen, B. Cai, X. Li, Enhanced particle swarm optimization based on network structure for feature selection, Complex Intell. Syst. 11 (2025) 473, https://doi.org/10.1007/s40747-025-02088-0.

[35] M. Jain, V. Saihjpal, N. Singh, S.B. Singh, An Overview of Variants and Advancements of PSO Algorithm, Appl. Sci. 12 (2022) 8392, https://doi.org/10.3390/app12178392.

[36] M. Hosseinzadeh, J. Tanveer, A.M. Rahmani, F.S. Gharehchopogh, N.M. Yusof, P. Khoshvaght, Z. Liu, T. Porntaveetus, S.-W. Lee, A Comprehensive Overview of PSO-LSTM Approaches: applications, Analytical Insights, and Future Opportunities, Arch Computat Methods Eng (2025), https://doi.org/10.1007/s11831-025-10445-y.

[37] M. Clerc, J. Kennedy, The particle swarm - explosion, stability, and convergence in a multidimensional complex space, IEEE Trans. Evol. Computat. 6 (2002) 58–73, https://doi.org/10.1109/4235.985692.
[38] Y. Tuppadung, W. Kurutach, Comparing nonlinear inertia weights and constriction factors in particle swarm optimization, KES 15 (2011) 65–70, https://doi.org/10.3233/KES-2010-0211.
[39] D. Lu, Y. Qiulu, W. Hao, H. Yiming, Q. Hefei, W. Huan, Z. Lingjuan, W. Wei, Review of Semiconductor distributed Feedback Lasers in the Optical Communication Band, Chin. J. Laser 47 (2020) 0701001, https://doi.org/10.3788/CJL202047.0701001.
[40] F.J. Galdieri, T. Sutili, N. Melnikoff, A.C. Bordonalli, E. Conforti, Influence of exterior acoustic noise on narrow linewidth laser measurements using self-homodyne optical fiber interferometer, Optik 204 (2020) 164101, https://doi.org/10.1016/j.ijleo.2019.164101.